Molecular Biology of the Cell
Vol. 15, 3475–3484, July 2004

Rho Kinase Regulates the Intracellular Micromechanical Response of Adherent Cells to Rho Activation

Thomas P. Kole,* Yiider Tseng,*‡ Lawrence Huang,† Joseph L. Katz,* and Denis Wirtz*‡§

*Department of Chemical and Biomolecular Engineering and †Department of Biomedical Engineering; and §Graduate Program in Molecular Biophysics, The Johns Hopkins University, Baltimore, Maryland 21218

Submitted March 15, 2004; Revised April 16, 2004; Accepted May 3, 2004
Monitoring Editor: Paul Matsudaira

Local sol-gel transitions of the cytoskeleton modulate cell shape changes, which are required for essential cellular functions, including motility and adhesion. In vitro studies using purified cytoskeletal proteins have suggested molecular mechanisms of regulation of cytoskeleton mechanics; however, the mechanical behavior of living cells and the signaling pathways by which it is regulated remains largely unknown. To address this issue, we used a nanoscale sensing method, intracellular microrheology, to examine the mechanical response of the cell to activation of the small GTPase Rho. We observe that the cytoplasmic stiffness and viscosity of serum-starved Swiss 3T3 cells transiently and locally enhances upon treatment with lysophosphatidic acid, and this mechanical behavior follows a trend similar to Rho activity. Furthermore, the time-dependent activation of Rho decreases the degree of microheterogeneity of the cytoplasm. Our results reveal fundamental differences between intracellular elasticity and cellular tension and suggest a critical role for Rho kinase in the regulation of intracellular mechanics.

INTRODUCTION

Cytoskeletal rearrangements are closely correlated with key cellular processes such as cell shape changes during mitosis, the separation of daughter cells by the contractile ring during cytokinesis, cell–cell and cell–substrate interactions, transmembrane signaling, endocytosis, secretion, and motility (Schmidt and Hall, 1998). These processes involve the coordinated assembly, disassembly, cross-linking, and bundling of cytoskeletal filaments, which are mediated by auxiliary proteins and are believed to regulate the mechanical properties of the cell. In vitro studies using purified cytoskeletal proteins have suggested molecular mechanisms of regulation of cytoskeleton mechanics (Sato *et al*., 1987; Janmey *et al*., 1990; Pollard *et al*., 1992); however, the mechanical behavior of living cells and the molecular signaling pathways by which it is regulated remains largely unknown.

It is well established that members of the Rho family of small GTPases play a central role in cytoskeletal assembly and architecture (Ridley and Hall, 1992; Ridley *et al*., 1992; Nobes *et al*., 1995; Van Aelst and D'Souza-Schorey, 1997; Rottner *et al*., 1999; Bishop and Hall, 2000). The roles of Rho proteins in controlling actin filament dynamics and network organization are fairly well understood at the biochemical level (Ballestrem *et al*., 2001). However, fundamental questions still exist regarding the downstream intracellular mechanical response of the cytoskeleton to Rho GTPase activation (Heidemann and Wirtz, 2004). For instance, upon activation of Rho, what are the *intracellular* viscoelastic properties that modulate the intracellular transport of organelles and engineered particles (Suh *et al*., 2003), and how does Rho activation affect the ability of the cell to resist deformation? Using a novel functional assay, intracellular microrheology (Tseng *et al*., 2002b), we directly measure the micromechanical response of Swiss 3T3 fibroblasts subjected to Rho activation by lysophosphatidic acid (LPA) and examine the effects of LPA upon cytoplasmic microheterogeneity. Our results suggest a critical role for Rho kinase in regulating cell mechanics and illustrate fundamental differences between cellular tension and intracellular stiffness.

Article published online ahead of print. Mol. Biol. Cell 10.1091/mbc.E04–03–0218. Article and publication date are available at www.molbiolcell.org/cgi/doi/10.1091/mbc.E04–03–0218.

‡ Corresponding authors. E-mail address: wirtz@jhu.edu and yiider@jhu.edu.

MATERIALS AND METHODS

Cell Culture and Reagents

Swiss 3T3 fibroblasts (American Type Culture Collection, Manassas, VA) were cultured in DMEM supplemented with 10% bovine calf serum (American Type Culture Collection) and maintained at 37°C in a humidified, 5% CO_2 environment. All intracellular microrheology (ICM) measurements were performed in an incubator mounted on an inverted microscope maintained at 37°C with 5% CO_2 and humidity. Cells were grown on 35-mm glass-bottom dishes coated with poly-D-lysine (MatTek, Ashland, MA) and treated with 50 μg/ml fibronectin (Calbiochem, San Diego, CA) for 1 h before plating. Cells were serum-starved in DMEM for 42 to 48 h before data collection. Inhibitor experiments were performed by treating cells with DMEM containing staurosporine (Sigma-Aldrich, St. Louis, MO) or Y-27632 (Calbiochem) at the specified final concentrations for 15 min before treatment with DMEM containing 1 μg/ml lysophosphatidic acid (Sigma-Aldrich) and data collection.

Cytomechanics from Multiple Particle Tracking

To measure the local mechanical properties of cytoplasm, we used the method of intracellular microrheology introduced by Tseng *et al*. (2002b). Yellow-green fluorescent carboxylate-modified polystyrene microspheres (0.1 μm; Molecular Probes, Eugene, OR) in Dulbecco's phosphate-buffered saline (DPBS; Invitrogen, Carlsbad, CA) were microinjected into cells and used as local probes of cytoplasm.

Microinjected cells containing fluorescent particles were placed on the stage of a microscope at 37°C. Movies of the fluctuating fluorescent microspheres were recorded onto the random-access memory of a PC computer via a silicon-intensifier target camera (VE-100; Dage-MTI, Michigan City, IN) mounted on an inverted epifluorescence microscope (Eclipse TE300; Nikon, Melville, NY) at a frame rate of 30 Hz by using the software Metavue (Universal Imaging, West Chester, PA). A 100× Nikon Plan Fluor oil-immersion objective (numerical aperture [NA] 1.3) was used for particle tracking, which permitted ~5-nm spatial resolution over a 120 × 120-μm field of view, as assessed by monitoring the apparent displacement of microspheres firmly attached to a glass coverslip with the same microscope and camera settings as used during the live cell experiments. The displacements $[x(t),y(t)]$, where t is the elapsed time, of the particles centroids were simultaneously monitored in the focal plane of the microscope for 20 s. The few particles that seemed to undergo "ballistic" or directed motions were ignored. At least 120 particle trajectories were measured for each experimental condition.

Movies of fluctuating microspheres were analyzed by a custom particle tracking routine incorporated into the MetaMorph imaging suite (Universal Imaging) as described previously (Tseng and Wirtz, 2001). Individual time-averaged mean square displacements (MSDs),

$$\langle \Delta r^2(\tau) \rangle = \langle [x(t+\tau) - x(t)]^2 + [y(t+\tau) - y(t)]^2 \rangle$$

where τ is the time scale, were calculated from the two-dimensional trajectories of the centroids of the microspheres. All control experiments are described in Tseng *et al*. (2002b), including effects of particle size and surface chemistry.

Particles embedded in the cytoplasm of living cells can be thought of as nano-scale rheometers that impose a time-averaged stress on the surrounding fluid on the order of k_BT/a^3 where k_B is the Boltzmann constant, T is the absolute temperature, and a is the particle radius. The resulting strain is measured as the particle displacement and can be directly related to the creep compliance, $\Gamma(\tau)$, of the surrounding fluid through the following relationship (Xu *et al*., 1998a):

$$\Gamma(\tau) = \frac{3k_BT}{2\pi a}\langle \Delta r^2(\tau) \rangle$$

The creep compliance is the ratio of the time-evolving strain to the time-averaged stress imposed by the probe particle, and is a measure of cell deformability. It shares all of the same features as the MSD so that a perfectly viscous fluid will have a time scale-dependent creep compliance with a power law slope of 1 whereas a perfectly elastic solid will have a power law slope of 0 (Xu *et al*., 1998).

All of the mechanical information is contained in the amplitude and the time scale dependence of the creep compliance. However, using the generalized form of the Stokes-Einstein relationship (Mason and Weitz, 1995)

$$G(s) = \frac{2k_BT}{3\pi a s \langle \Delta r^2(s) \rangle}$$

we can approximate the viscoelastic spectrum $G(s)$, where s is the Laplace frequency, from $\langle \Delta r^2\ (s) \rangle$, the unilateral Laplace transform of $\langle \Delta r^2\ (\tau) \rangle$. Using this expression, we can calculate the traditional frequency-dependent elastic modulus $G'(\omega)$ and loss modulus $G''(\omega)$ from time scale-dependent MSDs as described previously (Mason *et al*., 1997; Dasgupta *et al*., 2002). The viscoelastic moduli $G'(\omega)$ and $G''(\omega)$ are the real and imaginary parts, respectively, of the complex modulus $G^*(\omega)$, which is the projection of $G(s)$ in Fourier space, and obey Kramers-Kronig relationships (Mason *et al*., 1997). Viscoelastic moduli obtained from our particle-tracking approach quantitatively compare with bulk moduli measured using a classical rheometer (Mason *et al*., 1997). The error between the two types of measurements never exceeded 20%. It has been suggested that measurement of viscoelastic moduli by using particle tracking methods can be improved by monitoring the correlated motion between two particles instead of the motion of individual particles (Crocker *et al*., 2000). However, in its present form, this method is inappropriate for the measurement of the mechanical properties of live cells because it incorrectly assumes that the intracellular milieu is homogeneous. Furthermore, to obtain statistically significant measurements, data collection times are on the order of 30–60 min. Cells cannot be assumed as structurally stationary on this time scale because cytoskeletal filaments turn over on the order of tens of seconds to minutes (Theriot and Mitchison, 1991; McGrath *et al*., 1998).

The diffusion coefficient, D, of a microsphere of radius a can be calculated from the Stokes-Einstein relationship (Einstein, 1905; Chandrasekhar, 1943; Qian *et al*., 1991; Berg, 1993):

$$D = \frac{k_BT}{6\pi a \eta}$$

where η is the shear viscosity of the fluid surrounding the particle. In a viscoelastic fluid, such as the cytoplasm of a living cell, η is not a constant and is time scale dependent, thereby giving rise to a time scale-dependent diffusion coefficient. We can however instead approximate η as the product of the relaxation time (the time scale at which the viscous to elastic crossover occurs; Figure 2) and the plateau value of the elastic modulus (Eckstein *et al*., 1998). It is important to note that the diffusion coefficient calculated from two-dimensional particle trajectories can be approximated as the three-dimensional diffusion coefficient assuming that the local environment surrounding each microsphere is isotropic in three dimensions. We simply have

$$\langle \Delta r^2(\tau) \rangle_{2D} = \frac{2}{3}\langle \Delta r^2(\tau) \rangle_{3D}$$

This is a valid approximation, even in regions of the cell where long-range interactions between microspheres and the cell membrane could occur via hydrodynamic interactions, because those interactions are screened to within a mesh size of the surrounding network, which is ~50 nm. If the cell thickness were similar or smaller than the particle diameter, they would be mostly excluded from those thin regions.

Fluorescence Microscopy

Fluorescence microscopy was used to illustrate the heterogeneous organization of the actin cytoskeleton and spatial distribution of vinculin in Swiss 3T3 cells. Cells were fixed in 3% paraformaldehyde in DPBS and permeabilized in 0.1% Triton X-100 (Sigma-Aldrich) in DPBS. Cells were blocked in 10% fetal bovine serum for 30 min and labeled with a vinculin monoclonal antibody (mAb) at 1:100 (Sigma-Aldrich) dilution for 1 h at room temperature. Cells were subsequently labeled with Alexa 488 phalloidin at 1:40 (Molecular Probes) and Alexa 540 anti-mouse 1:50 (Molecular Probes) for 1 h at room temperature. Coverslips were mounted in Antifade (Molecular Probes) to minimize photobleaching. Fluorescently labeled cells were observed with a 60×, oil immersion objective (NA 1.4) mounted on a Nikon Eclipse TE300 inverted microscope. Images were acquired with a PCM2000 laser scanning confocal microscope (Nikon) or an Orca II charge-coupled device camera (Hamamatsu, Bridgewater, NJ) controlled by the Metavue software (Universal Imaging).

Phase Contrast Microscopy

The subcellular organization and morphology of live cells were revealed using phase contrast microscopy via a 60× oil-immersion Plan Fluor lens (NA 1.4) (Nikon). This lens was mounted on a Nikon Eclipse TE300 inverted microscope. Images were acquired with an Orca II CCD camera (Hamamatsu) controlled by the Metavue software (Universal Imaging).

Rho Activity Measurements

Rho activity was measured using the pull-down assay developed by Ren *et al*. (1999) and Ren and Schwartz (2000). The Rho-binding domain (RBD) from Rhotekin was expressed and isolated in *Escherichia coli* by using a plasmid kindly provided by Dr. X.D. Ren and immobilized on Sepharose 4B (Amersham Biosciences UK, Little Chalfont, Buckinghamshire, United Kingdom). Swiss 3T3 cultures were lysed in cold lysis buffer (50 mM Tris, pH 7.2, 1% Triton X-100, 0.5% sodium deoxycholate, 0.1% SDS, 500 mM NaCl, 10 mM $MgCl_2$, 10 μg/ml each of leupeptin and aprotinin, and 1 mM phenylmethylsulfonyl fluoride) and incubated at 4°C with immobilized RBD for 1 h. Samples were analyzed by SDS-PAGE and visualized on Western blots by using mAbs against RhoA (Santa Cruz Biotechnology, Santa Cruz, CA). Rho activity was determined as the amount of RBD-bound Rho versus total Rho in the lysate by densitometry analysis of the blots by using Un-Scan-It gel software (Silk Scientific, Orem, UT).

RESULTS

Cytomechanical Response to Rho Activation

To investigate the effects of Rho activation on the mechanical properties of living cells, we used a new method, ICM, to probe in situ the local viscoelastic properties of quiescent Swiss 3T3 cells before and after treatment with the known Rho agonist LPA (Ridley and Hall, 1992; Moolenaar, 1995). This force-free method transforms the measured Brownian displacements of individual microspheres embedded in the cytoplasm into local viscous and elastic moduli as described previously (Mason *et al*., 1997; Apgar *et al*., 2000; Dasgupta *et al*., 2002). The time-dependent coordinates of the centroids of individual 0.1-μm-diameter microspheres were tracked using time-resolved video fluorescence microscopy with ~5-nm spatial resolution and 33-ms temporal resolution (Figure 1, A and B). Particle trajectories were then transformed into time-averaged MSDs, compliance (i.e., cell deformability) profiles (Figure 2A), and frequency-dependent viscoelastic moduli (Figure 2B). Details about the method of

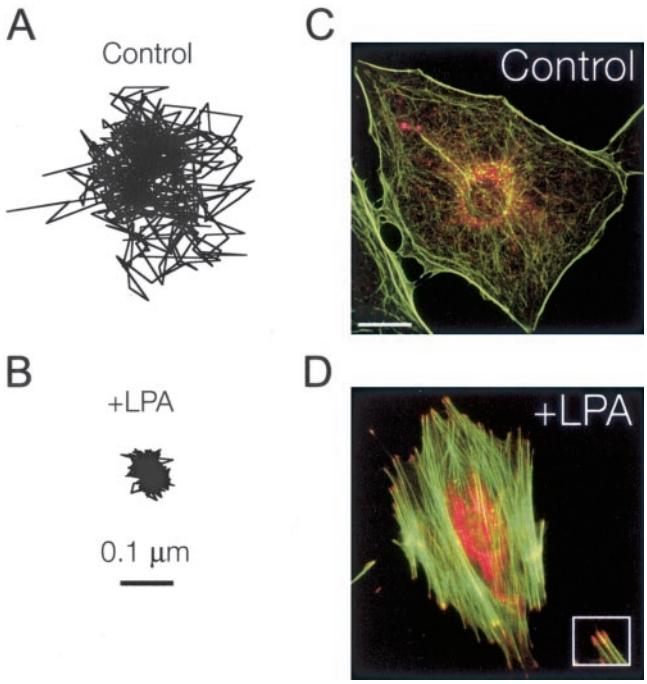

Figure 1. Motion of particles embedded in the cytoplasm. (A and B) Typical trajectories of microspheres injected into the cytoplasm of serum-starved Swiss 3T3 cells before (A) and 15 min after (B) treatment with 1 μg/ml LPA. Scale bar indicates length scale for both trajectories. (C and D) Fluorescent micrographs of serum-starved Swiss 3T3 cells before (C) and 15 min after (D) treatment with 1 μg/ml LPA. Actin filaments (*green*) were visualized with Alexa 488 phalloidin, whereas focal adhesion complexes (red) were visualized with a mAb against vinculin and Alexa 566 goat anti-mouse. Bar, 20 μm. Inset, magnified view of focal adhesions at the ends of actin stress fibers.

ICM can be found in Tseng *et al*. (2002b), which offers a thorough description of control experiments involving microspheres of different size and surface charge.

The extent of the displacements of microspheres embedded in the cytoplasm of Swiss 3T3 cells treated with LPA was much smaller than that of control cells (Figure 1, A and B), suggesting that the microenvironment surrounding the microspheres was significantly stiffer in Rho-activated cells. This was further evidenced by a large decrease in the magnitude of the cellular compliance (i.e., deformability) of the cytoplasm at all time scales upon treatment with LPA (Figure 2A) and coincided with the formation of organized F-actin structures, including stress fibers and focal adhesions (Figure 1, C and D). To test the statistical significance of the differences observed in the creep compliance of control and LPA-treated cells, we applied two-tailed *t* tests at each time scale from 0.033 to 10 s and averaged their values to obtain an average p value of < 0.05. To test whether the observed micromechanical response was in part due to activation of Rho, control experiments were performed using quiescent 3T3 cells microinjected or treated with 10 μg/ml C3 transferase (a potent inhibitor of the downstream functions of active Rho) before treatment with LPA. Cells treated with C3 displayed different morphologies than normal quiescent cells (our unpublished data) with a slightly lower baseline mean cellular compliance (Figure 2A, inset); however, after 15 min of treatment with 1 μg/ml LPA there were no significant changes in the mean creep compliance (Figure 2A, inset), average p value = 0.6. This result suggests that the observed micromechanical effects of LPA are due to the activation of Rho and not another signaling pathway that may be activated by LPA.

The local elastic and loss (viscous) moduli, $G'(\omega)$ and $G''(\omega)$ (Figure 2B), of the cytoplasm were directly obtained via the analytical continuation of the generalized form of the Stokes-Einstein relationship into the Fourier domain and approximation of the frequency dependent MSD as described previously (Mason *et al*., 1997; Dasgupta *et al*., 2002). $G'(\omega)$ and $G''(\omega)$, respectively, characterize the elasticity (i.e., the propensity of the cytoplasm to rebound after a force is applied) and the viscosity of cytoplasm. The elasticity G' of the cytoplasm in both control cells and LPA-treated cells exhibited steep frequency dependence at low frequencies before reaching a quasi-plateau at intermediate and high frequencies (Figure 2B). The plateau value of the elasticity in LPA-treated cells was nearly twice that of control cells. These results contrast those obtained using a twisting magnetic bead technique where the elasticity of endothelial cells was shown to decrease in response to treatment with LPA (Bausch *et al*., 2001). This discrepancy may be due to the difference in cell types or the fact that the later technique probes the mechanics of the cell membrane and not intracellular mechanics.

The loss modulus G'' of the cytoplasm dominated the elastic modulus G' at low frequencies, became smaller than G' at intermediate frequencies and comparable with G' at high frequencies for both control cells and LPA-treated cells (Figure 2B). This type of frequency profile for G' and G'' suggests that the cytoplasm behaves as a viscoelastic solid ($G' > G''$) at high rates of deformation and as a viscoelastic liquid ($G' < G''$) at low rates of deformation. This is clearly shown by the behavior of the phase angle or loss tangent (Figure 2C), $\delta = \arctan(G''/G')$, which is nearly 90° (perfectly viscous liquid) at low frequencies and then begins to rapidly decrease with increasing frequency. In LPA-treated cells, the loss tangent crosses over to the elastic regime ($\delta < 45°$) at a much lower frequency than control cells (Figure 2C), suggesting that activation of Rho enables the cell to elastically resist a wider range of rates of deformations compared with quiescent cells. These viscoelastic profiles, which are reminiscent of those found in polymeric fluids (Ferry, 1980) and reconstituted actin networks cross-linked with α-actinin (Sato *et al*., 1987; Xu *et al*., 1998b), describe the cytoplasm as a complex fluid that when sheared rapidly, resists deformations and is therefore elastic, and when sheared slowly, relaxes rapidly via viscous diffusion and thereby offers less resistance to mechanical stresses.

Intracellular viscosity is obtained from the product of the relaxation time (inverse of the cross-over frequency, $\tau_{\delta=45°}$) and the plateau modulus (the value of the elastic modulus evaluated at the frequency where the minimum of δ occurs) (Eckstein *et al*., 1998). Intracellular viscosity increased from 8.1 ± 10.0 to 94.1 ± 22.1 Poise upon Rho activation (Figure 2D). This viscosity governs the rate of transport of organelles and particles larger than the effective mesh size of cytoplasm (>50 nm). It is much higher than measured by fluorescence recovery after photobleaching, which measures the interstitial viscosity of cytoplasm (~0.01 Poise) (Luby-Phelps, 1993, 2000). The mean diffusion coefficient of the microspheres before and after LPA treatment, $D = 5.59 \times 10^{-3}$ and 0.48×10^{-3} μm^2/s, was obtained from the Stokes-Einstein relationship by using the calculated shear viscosity (Figure 2D) of control and LPA-treated cells (see MATERIALS AND METHODS). These values for the diffusion coefficient suggest that the intracellular transport of 0.1-μm particles is hindered >10-fold upon activation of Rho.

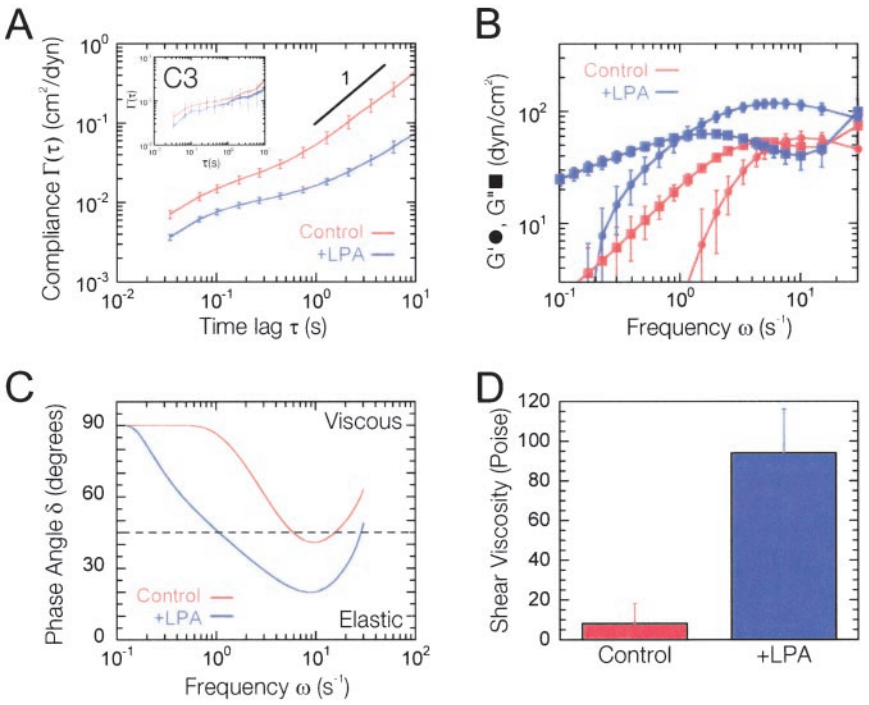

Figure 2. Cytomechanical response of Swiss 3T3 cells to Rho activation. (A) Mean cellular compliance directly computed from the mean-squared displacements of the thermal motions of microspheres injected into the cytoplasm of serum-starved Swiss 3T3 cells before (red) and 15 min after (blue) treatment with 1 μg/ml LPA. Error bars denote SE of measurement. Inset, mean cellular compliance of the cytoplasm of serum-starved Swiss 3T3 cells injected with 10 μg/ml C3, before (red) and after (blue) treatment with 1 μg/ml LPA. (B) Frequency-dependent viscous and elastic moduli, $G''(\omega)$ and $G'(\omega)$, obtained from mean cellular compliances (A). $G'(\omega)$ is represented by circles and $G''(\omega)$ by squares. (C) Frequency-dependent phase angle, $\delta = \arctan(G''/G')$, calculated from viscoelastic moduli (B). (D) Shear viscosity obtained from the product of the plateau modulus and relaxation time (B).

Effect of Rho Activation on Cytoplasmic Microheterogeneity

Quiescent and LPA-treated Swiss 3T3 cells may differ not only in their global mechanical behavior but also in their spatial distribution of local moduli. To illustrate the mechanical microheterogeneity of the cells, microspheres were color-coded between red (soft) and blue (stiff) according to the local value of cellular compliance and superimposed on a phase contrast micrograph of the cell (Figure 3A). Figure 3 shows that the micromechanical behavior of the cytoplasm of both control and LPA-treated cells was heterogeneous and that all probed regions of the cytoplasm stiffened in response to LPA treatment. These results are consistent with the observed global reorganization of F-actin structures within the cell upon activation of Rho (Figure 3D) as opposed to localized actin reorganization as found with other Rho GTPases (e.g., Cdc42 and Rac) (Ridley and Hall, 1992; Ridley *et al*., 1992; Kozma *et al*., 1995). From Figure 3, D and E, it is also apparent that there is little correlation between local F-actin bundle organization and the local viscoelastic properties of the cell. Blue colored (stiff) particles occur in regions where F-actin staining is mostly absent, whereas red colored (soft) particles can be found in the most intense F-actin regions.

Analysis of the normalized local cellular compliance (local cellular compliance divided by the mean cellular compliance) at time scales of 0.1 and 1 s shows that the distribution of stiffness is less spread (lower variance) after application of LPA (Figure 3, B and C). However, the direct comparison of the shape of distributions that have different means may be somewhat misleading when one only considers absolute statistical parameters such as skewness and variance. Therefore, we introduced markers to quantify the relative degree of micromechanical heterogeneity of the cytoplasm of living cells: the relative contributions of the 10, 25, and 50% highest compliance values to the mean compliance (Figure 4B). These contributions should be exactly 10, 25, and 50% for a perfectly homogeneous liquid, which is what we observed when 1-μm-diameter, particles were dispersed in a homogenous aqueous solution of glycerol (Figure 4A). These markers should become close to 100% in a highly heterogeneous milieu, which is what is observed, for example, in a highly heterogeneous actin filament network in the presence of a high concentration of the F-actin cross-linking protein α-actinin (Tseng and Wirtz, 2001) and fascin (Apgar *et al*., 2000) and in concentrated DNA solutions (Goodman *et al*., 2002). Here, we found that the contributions of the 10, 25, and 50% highest compliance values to the mean compliance of quiescent Swiss 3T3 cells treated with 1 μg/ml LPA were significantly lower than those of control cells. However, both sets of contributions were more than twice as high as those measured in glycerol (Figure 4A), which is expected given the heterogeneous nature of the actin cytoskeleton (Figure 1, C and D), a major contributor to cell viscoelasticity (Yamada *et al*., 2000). These results suggest that activation of Rho decreases the degree of heterogeneity of the cytoplasm, potentially by the homogenization of actin structures, and are in agreement with the near fourfold decrease in the variance of the normalized cellular compliance (3.52–0.93) of the cellular compliance of the cell upon addition of LPA.

Time-dependent Micromechanics of Rho Activation

To explore the time-dependent micromechanical response of the cytoplasm to Rho activation, we measured the mechanical properties of quiescent Swiss 3T3 cells as a function of time after LPA treatment (Figure 5, A and B). On treatment with LPA, the mean compliance of the cells (Figure 5A, inset) initially decreased describing a stiffening of the cytoplasm as evidenced by the sharp increase in both the plateau modulus and shear viscosity. The plateau modulus of the cytoplasm reached a maximum of 117 ± 10 dyn/cm^2, 15 min after application of LPA (Figure 5B). This enhancement in cytoplasmic stiffness was followed by a relaxation; cytoplasmic elasticity approached pretreatment, basal G' levels after 60 min (Figure 5B). The microheterogeneity of the cell follows a trend similar to that of intracellular stiffness, reaching

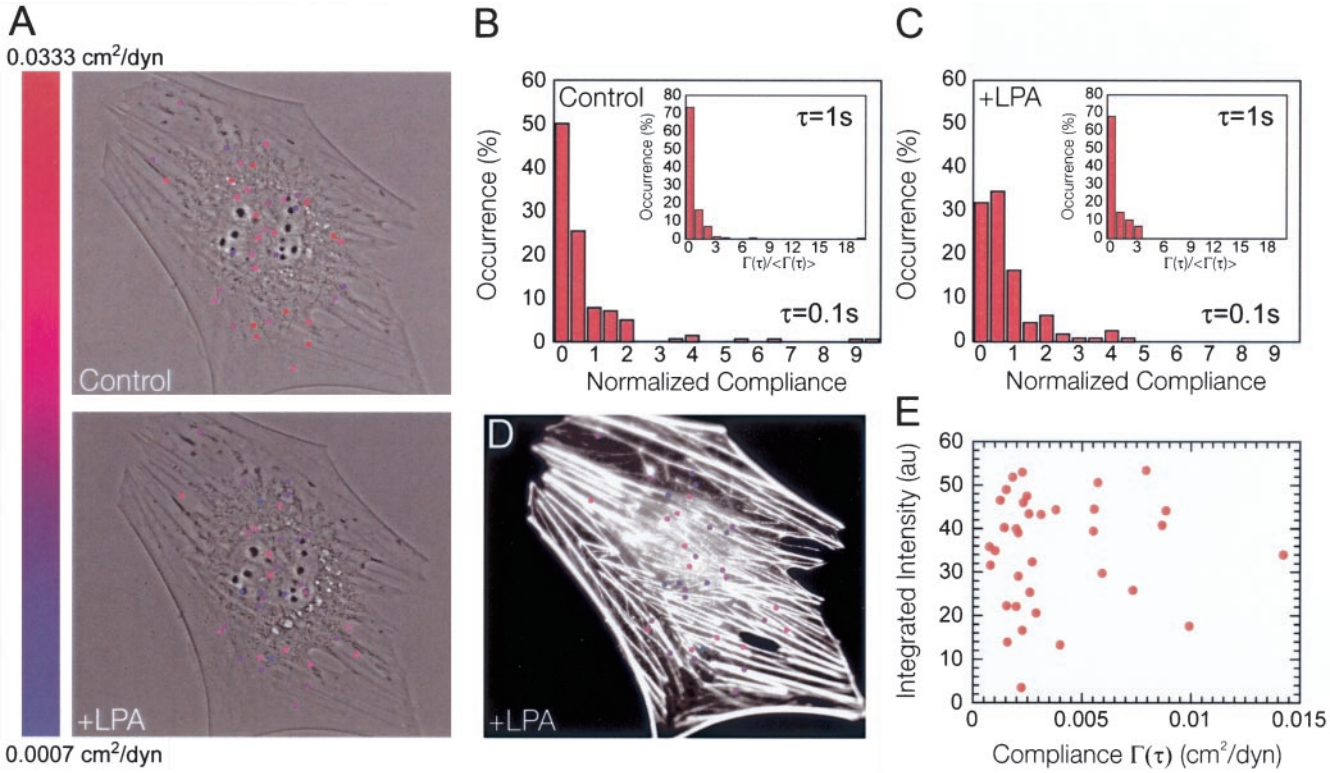

Figure 3. Effect of LPA treatment on the microheterogeneity of the cytoplasm. (A) Phase contrast micrographs of a serum-starved Swiss 3T3 cell overlaid with fluorescent micrographs of fluorescent microspheres injected into the cytoplasm before and 15 min after treatment with 1 μg/ml LPA. Here, we only show tracked particles and have neglected aggregates that violate assumptions made in the generalized Stokes-Einstein relationship. Each particle position was color-coded corresponding to the local value of the cellular compliance at that position in the cell at a time scale of 1 s. Note that the color indicators at each particle position do not reflect the size of the particle (0.1 μm). Indicator size was increased to aid visual presentation. (B and C) Distribution of local cellular compliances within the cytoplasm of serum-starved Swiss 3T3 cells before (B) and 15 min after (C) treatment with 1 μg/ml LPA measured at a time scale of 1 s. Inset, subcellular distribution of local cellular compliance measured at a time scale of 0.1 s. (D) Fluorescent micrograph of the cell shown in (A) overlaid with fluorescent micrographs of fluorescent microspheres injected into the cytoplasm. The cell was fixed 15 min after treatment with 1 μg/ml LPA and stained with Alexa 566 phalloidin to visualize actin filaments (white). Each particle position was color coded as described above. (E) F-actin bundle intensity integrated over the area covered by each particle region displayed in A and plotted against the local value of the cellular compliance at a time scale of 1 s.

a minimum degree of heterogeneity at 15 min, as indicated by contributions of the 10, 25, and 50% highest compliance values to the mean compliance (Figure 6). In striking contrast to these cytomechanics measurements, fluorescent micrographs of the actin cytoskeleton revealed that Rho-induced F-actin bundles and focal adhesions remained well established during the entire course of the experiment (Figure 5D). These experiments indicate that the cell's mechanical response to Rho activation is transient and suggest that the level of subcellular stiffness does not necessarily correlate with the presence of F-actin bundles and focal adhesions displayed in fluorescence micrographs.

The transient mechanical response of cytoplasm follows the time-dependent activity of Rho by LPA/serum treatment (Ren *et al*., 1999) with a delay (Figure 5, B and C). Using a pull-down assay based on specific binding of GTP-bound Rho to the Rho-binding domain from the effector Rhotekin (Ren *et al*., 1999), we measured the activity of Rho as a function of time in conditions identical to those used in ICM experiments. We found that upon treatment with LPA, Swiss 3T3 cells underwent a rapid increase in Rho activation that reached a maximum at 1 min. These cells then experienced a rapid decrease in Rho activity that approached basal levels within 3 min (Figure 5, B and C). Similar results were reported by Ren *et al*. (1999); however, they observed a peak in Rho activity at 3 min. It has been suggested that the transient activation of Rho is due to a negative-feedback loop that includes the activation of proteins known to antagonize Rho such as p190RhoGAP (Arthur and Burridge, 2001) or one of the other members of the Rho GTPase family, such as Rac or Cdc42 (Ren *et al*., 1999). Together, cytomechanics experiments and pull-down assay results show that Rho-induced cell stiffening is transient and that cell stiffening parallels, with a delay, the time-dependent activity of Rho.

Rho Kinase Regulates the Cytomechanical Response to Rho Activation

Active Rho is known to act through the combined efforts of the Rho effectors ROCK/Rho-associated kinase (Amano *et al*., 1996; Kimura *et al*., 1996) and Dia (Watanabe *et al*., 1999) but may include other targets such as phosphatidylinositol-4-phosphate 5-kinase (Ren *et al*., 1996; Hall, 1998). Rho kinase stimulates myosin-dependent contraction of the actin cytoskeleton by directly inhibiting myosin light chain phosphatase and indirectly activating myosin light chain kinase (Kaibuchi *et al*., 1999). This results in the bundling of actin filaments into stress fibers and the clustering of integrin

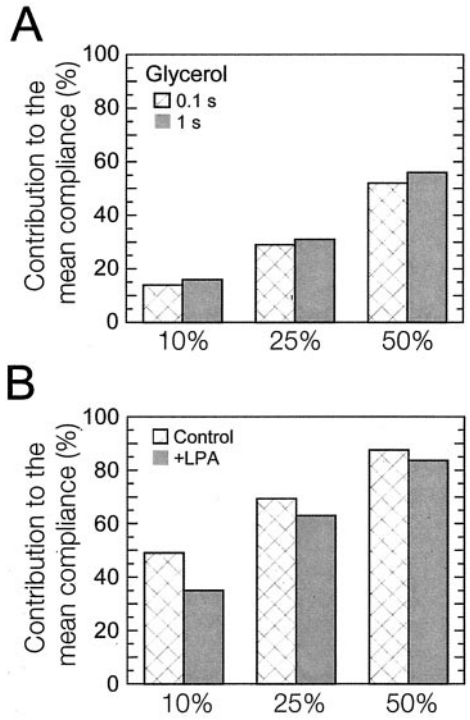

Figure 4. Statistical analysis of cellular compliance distributions. (A) Percentage of contributions of the highest 10, 25, and 50% values of local compliance to the mean compliance in a glycerol solution measured at a time scale of 0.1 s (first columns) and 1.0 s (second columns). These contributions are close to the expected values for a perfectly homogeneous solution, i.e., 10, 25, and 50%. (B) Contributions of the highest 10, 25, and 50% values of local compliance to the mean compliance of quiescent Swiss 3T3 cells before (first columns) and after (second columns) treatment with 1 μg/ml LPA.

complexes into focal adhesions (Chrzanowska-Wodnicka and Burridge, 1996), leading to cellular tension. Focal adhesions are critical sites of signal transduction and upon formation lead to the phosphorylation of key signaling proteins such as focal adhesion kinase (FAK), paxillin, and c-Src (Hanks *et al*., 1992; Seufferlein and Rozengurt, 1994; Arthur *et al*., 2000). FAK, paxillin, and c-Src have been shown to contribute to integrin mediated down-regulation of Rho (Arthur *et al*., 2000; Ren *et al*., 2000; Tsubouchi *et al*., 2002), and recent studies suggest that they may act through interaction with the Rho antagonist p190RhoGAP (Masiero *et al*., 1999; Arthur *et al*., 2000; Arthur and Burridge, 2001).

To discern the effects of contractility and focal adhesion formation on the cytomechanical response of LPA-treated quiescent Swiss 3T3 cells, we first performed ICM measurements in cells pretreated with the wide-spectrum kinase inhibitor staurosporine (Figure 7, A and B). Staurosporine blocked the LPA-induced formation of stress fibers and focal adhesions while preserving actin polymerization (Figure 7C) (Nobes and Hall, 1995). Previous studies using Swiss 3T3 fibroblasts plated on flexible silicon rubber substrates showed that treatment of cells with staurosporine completely abrogated Rho induced cellular tension (Ballestrem *et al*., 2001). In contrast to these observations, our cytomechanics assay revealed that the activation of Rho in staurosporine-treated cells resulted in cytoplasmic stiffening as evidenced by the decrease in the mean cellular compliance of the cytoplasm (Figure 7A, inset). Cytoplasmic stiffness no longer relaxed but rather reached a quasi steady-state plateau after 30 min as shown by the time-dependent plateau modulus profile of cells treated with LPA and staurosporine (Figure 7B). Remarkably, this final value of cytoplasmic stiffness (121 $\pm$ 15 dyn/cm^2) was nearly identical to that obtained at the peak of cell stiffness in cells treated with LPA alone (117 $\pm$ 10 dyn/cm^2) (Figures 5B and 7B). These results suggest that even when actomyosin contractility is inhibited, cell stiffening can still occur presumably due to unaffected actin polymerization and the resulting formation of stiff F-actin networks (Tseng *et al*., 2002a). These results also underline the fundamental difference between cellular tension and intracellular stiffening.

A similar effect was observed in cells pretreated with the specific Rho kinase inhibitor Y-27632. Rho activation in Y-27632-treated cells resulted in the formation of F-actin structures without the development of contractile actin stress fibers or focal adhesions (Figure 8D). Previous studies have shown that Y-27632 prevents Rho-induced tyrosine phosphorylation of FAK and paxillin (Imamura *et al*., 2000; Sinnett-Smith *et al*., 2001). Although Y-27632 completely inhibited the contractile effects of Rho activation (Ballestrem *et al*., 2001; Riveline *et al*., 2001), the plateau modulus significantly increased (and, vice versa, the compliance decreased; Figure 8A, inset), reaching a quasi-plateau after 30 min with a value more than twice (255 $\pm$ 47 dyn/cm^2) that of the maximum elasticity obtained in control cells (Figures 5B and 8B). The distributions of compliance obtained by ICM were statistically analyzed by the contributions of the 10, 25, and 50% highest compliance values to the mean compliance. Cells pretreated with Y-27632 or staurosporine exhibited minimum degrees of heterogeneity upon activation of Rho that were lower than those of control cells and persisted for 60 min (see Supplementary Figure 1). This behavior follows a trend similar to Rho activity measured using the Rho pull-down assay with LPA- and Y-27632-treated cells (Figure 8, B and C). Together, these results and the observation that cell stiffness in control cells is transient, suggests that Rho kinase and/or the downstream myosin-dependent formation of focal adhesions not only plays a critical role in the regulation of Rho activity but also the cytomechanical response of Swiss 3T3 cells to Rho activation.

DISCUSSION

Through the use intracellular microrheology, we were able to probe the local intracellular mechanical properties of serum-starved Swiss 3T3 cells exposed to the known Rho agonist LPA. Quiescent Swiss 3T3 fibroblasts treated with LPA exhibit significant increases in both cytoplasmic elasticity and viscosity. The observed viscoelastic behavior is dynamic and deformation frequency dependent, which is similar to previous results found in cross-linked actin filament networks (Sato *et al*., 1987). The negative shift in the deformation frequency cross-over in LPA-treated cells indicates that the cytoskeleton becomes elastically responsive to a wider range of deformation frequencies. This may be due to the activation of one or more cross-linking proteins that possess lower actin dissociation rates, thus reducing the frequency of cross-linker rearrangement.

Our results further show that the mechanical response of Swiss 3T3 cells to Rho activation by LPA is time dependent and follows a trend similar to the time-dependent profile of Rho activity (Ren *et al*., 1999). This mechanical response is not instantaneous and is delayed with respect to Rho activation. Delayed stiffening of the cell may be attributed to the slow gelation kinetics of the networks of newly formed Rho-induced polymerized actin (Tseng *et al*., 2002a). In vitro

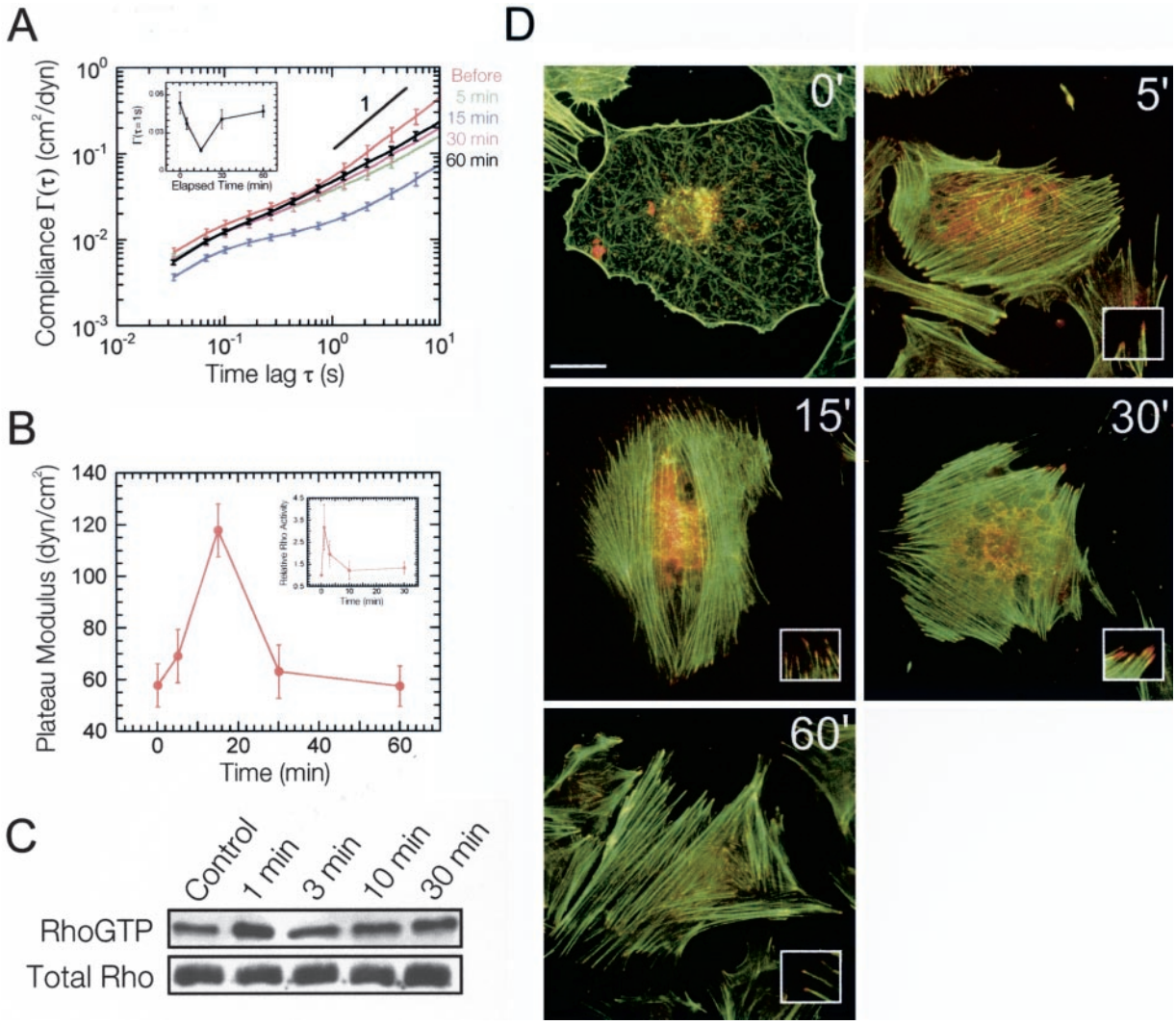

Figure 5. Kinetics of cytomechanical response of Swiss 3T3 cells to Rho activation. (A) Time-dependent mean cellular compliances directly computed from the mean-squared displacements of the thermal motions of microspheres injected into the cytoplasm of serum-starved Swiss 3T3 cells before and after treatment with 1 μg/ml LPA. Error bars denote SE of measurement. Inset, cellular compliance as a function of elapsed time at a time scale of 1 s. (B) Time-dependent plateau modulus obtained from mean cellular compliances before and after treatment with 1 μg/ml LPA. Inset, relative Rho activity obtained from Western blots of Rho pull-down experiments (C). Values are means obtained from three experiments ± SD. (C) Western Blot from one Rho pull-down experiment. (D) Time-dependent fluorescent micrographs of serum-starved Swiss 3T3 cells before and after treatment with 1 μg/ml LPA. Actin filaments (green) were visualized with Alexa 488 phalloidin, whereas focal adhesion complexes (red) were visualized with a mAb against vinculin and Alexa 566 goat anti-mouse. Bar, 20 μm. Inset, magnified view of focal adhesions at the ends of actin stress fibers.

studies using polymerized actin filaments and actin cross-linking proteins showed that the time required to reach a mechanical steady state (gelation time) is indeed long compared with the kinetics of actin polymerization or cross-linker binding (Tseng *et al.*, 2002a). Comparison of the observed micromechanical trends in control cells treated with LPA with fluorescent micrographs of the actin cytoskeleton shows that contrary to conventional wisdom, there is little correlation between F-actin structures and their mechanical function. Although LPA elicits rapid formation of actin stress fibers and global stiffening of the cell, micromechanical relaxation of the cell is not accompanied by disassembly of stress fibers and other organized F-actin bundles. This is supported by earlier observations in endothelial cells treated with thrombin where the mechanical properties of the cell membrane showed no correlation with the underlying organization of the actin cytoskeleton (Bausch *et al.*, 2001).

Previous studies have shown that down-regulation of Rho activity is necessary for focal adhesion turnover and cell migration (Ren *et al.*, 2000). Our results suggest that this requirement for cell motility may be due to the relaxation of intracellular stiffness, which we have shown to occur in response to LPA-induced activation of Rho in cultured Swiss 3T3 cells plated on fibronectin. This is further supported by the observation that treatment of Swiss 3T3 cells with the specific Rho kinase inhibitor Y-27632 abrogates the relaxation of the intracellular stiffness, resulting in a sustained, elevated stiffness that is more than twice that of control cells. Y-27632 has been shown to inhibit cellular migration and morphological changes in rat ascites hepatoma (MM1) cells

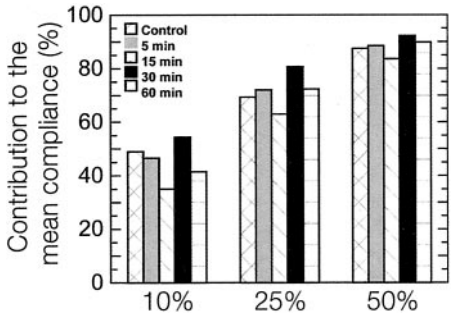

Figure 6. Time-dependent statistical analysis of cellular compliance distributions. Time-dependent percentage of contributions of the highest 10, 25, and 50% values of local compliance to the mean compliance of quiescent Swiss 3T3 cells before and after treatment with 1 μg/ml LPA.

through inhibition of Rho kinase-mediated tyrosine phosphorylation of FAK and paxillin (Imamura *et al*., 2000).

The observed enhancement of intracellular stiffness upon activation of Rho in quiescent Swiss 3T3 cells pretreated with Y-27632 or staurosporine also indicates that actin polymerization and the corresponding formation of entangled networks and bundles dominate intracellular stiffening, not actomyosin contractility and the formation of focal adhesions. The more than twofold difference in the peak elasticity of cells treated with staurosporine versus Y-27632 (121 vs. 255 dyn/cm^2) may result from the fact that the application of staurosporine prevents normal function of actin-cross-linking and actin-bundling proteins such as α-actinin and fascin (Tilney *et al*., 2000).

Another important aspect of this work is the distinction observed between intracellular stiffness and the cellular tension generated by myosin-based contraction of the actin cytoskeleton. Rho-induced cellular tension was recently observed using traction force microscopy with cells plated on semiflexible substrates (Ballestrem *et al*., 2001). The authors found that activation of Rho by LPA within these cells enhanced wrinkling of the underlying elastic substrate, which persisted for at least 60 min. Treatment of the same cells with Y-27632 or staurosporine resulted in complete disappearance of the wrinkles (Ballestrem *et al*., 2001), indicating that LPA induced acto-myosin contractility is critically dependent upon Rho kinase. Our intracellular microrheology assay reveals that activation of Rho in Y-27632–treated cells causes the intracellular stiffness to reach levels that are more than twice that of untreated cells. Together, these results define a key distinction between cellular tension and intracellular stiffness, both of which are critical in the control of cell motility.

This study has helped elucidate the contributions of focal adhesions and contractile stress fibers to cell stiffness, has suggested the fundamental difference between cellular tension and intracellular stiffness, and revealed the regulation

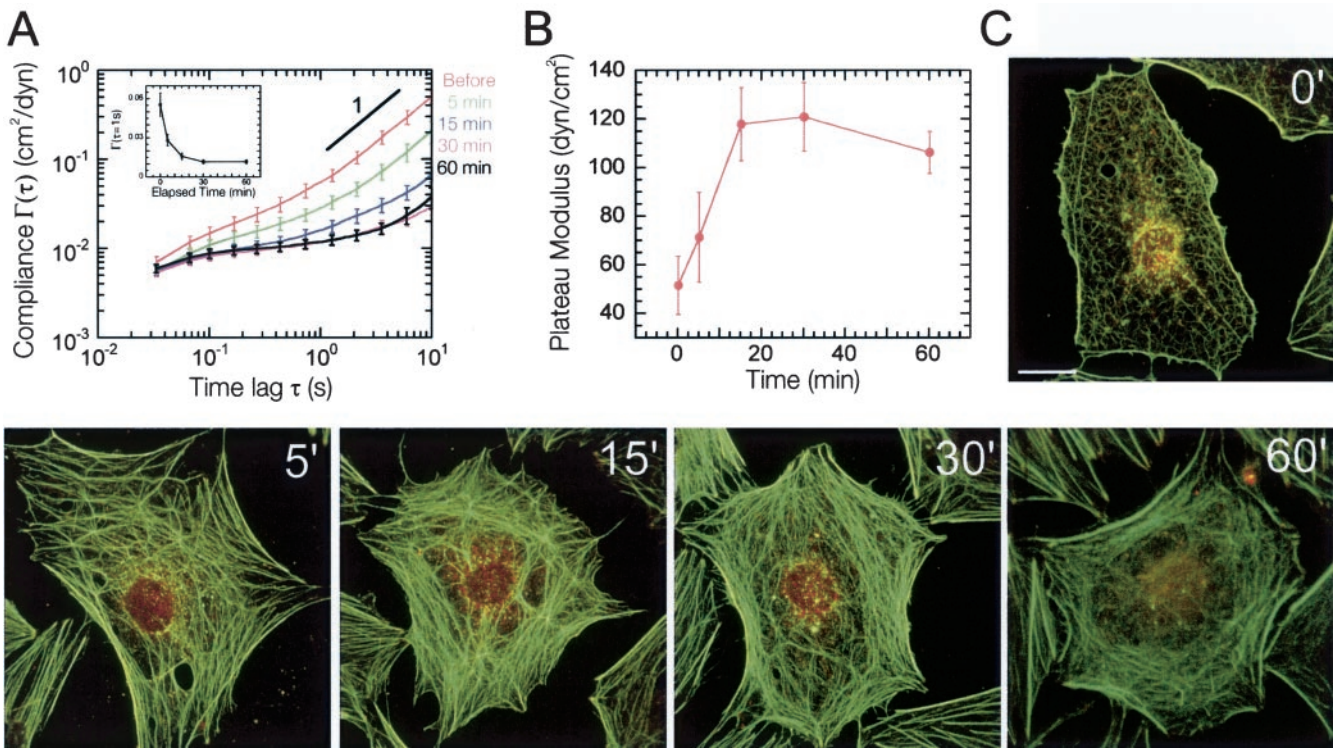

Figure 7. Cytomechanical response of Swiss 3T3 cells to Rho activation in the presence of Staurosporine. (A) Time-dependent mean cellular compliances directly computed from the mean-squared displacements of the thermal motions of microspheres injected into the cytoplasm of staurosporine (50 nM)-treated, serum-starved Swiss 3T3 cells before and after treatment with 1 μg/ml LPA. Error bars denote SE of measurement. Inset, cellular compliance as a function of elapsed time at a time scale of 1 s. B, time-dependent plateau modulus obtained from mean cellular compliances before and after treatment with 1 μg/ml LPA. (C) Time-dependent fluorescent micrographs of staurosporine-treated (50 nM), serum-starved Swiss 3T3 cells before and after treatment with 1 μg/ml LPA. Actin filaments (green) were visualized with Alexa 488 phalloidin, whereas focal adhesion complexes (red) were visualized with a mAb against vinculin and Alexa 566 goat anti-mouse. Bar, 20 μm.

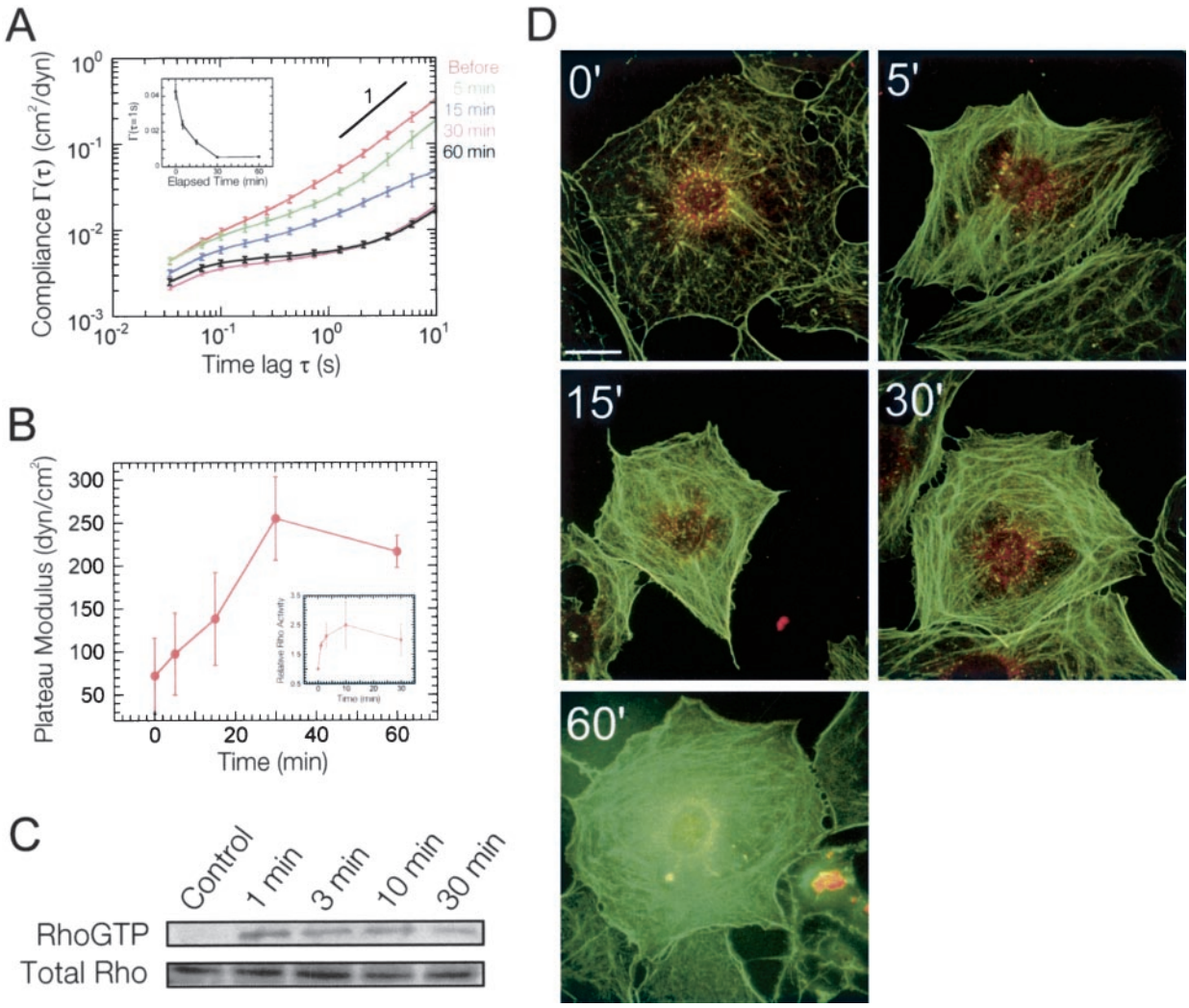

Figure 8. Cytomechanical response of Swiss 3T3 cells to Rho activation and Rho kinase inhibition. (A) Time-dependent mean cellular compliances directly computed from the mean-squared displacements of the thermal motions of microspheres injected into the cytoplasm of Y-27632 (10 μM)-treated, serum-starved Swiss 3T3 cells before and after treatment with 1 μg/ml LPA. Error bars denote SE of measurement. Inset, cellular compliance as a function of elapsed time at a time scale of 1 s. (B) Time-dependent plateau modulus obtained from mean cellular compliances (A). Inset, relative Rho activity (blue) obtained from Western blots of Rho pull-down experiments (C). Values are means obtained from four experiments ± SD. (C) Western Blot from one Rho pull-down experiment. (D) Time-dependent fluorescent micrographs of Y-27632 (10 μM)-treated, serum-starved Swiss 3T3 cells before and after treatment with 1 μg/ml LPA. Actin filaments (green) were visualized with Alexa 488 phalloidin, whereas focal adhesion complexes (red) were visualized with a mAb against vinculin and Alexa 566 goat anti-mouse. Bar, 20 μm.

by Rho kinase of the cytomechanical response to Rho activation by LPA. This work establishes a rigorous framework of how to functionally analyze the mechanical effects of activation of other prominent members of the Rho family of small GTPases, including Rac and Cdc42, which also mediate actin cytoskeleton reorganization.

ACKNOWLEDGMENTS

We thank Dr. A. Hall for helpful discussions, Dr. X.D. Ren for providing the expression plasmid for RBD, and Dr. M. Schwartz for help in the use of the Rho pull-down assay. This work was has been supported by National Institutes of Health and National Aeronautics and Space Administration grant NAG9-1563 (to D.W. and Y.T.) and National Science Foundation grant NES/NIRT CTS0210718 (to D.W.). T.P.K. was supported by a National Aeronautics and Space Administration training grant NGT965.

REFERENCES

Amano, M., Ito, M., Kimura, K., Fukata, Y., Chihara, K., Nakano, T., Matsuura, Y., and Kaibuchi, K. (1996). Phosphorylation and activation of myosin by Rho-associated kinase (Rho-kinase). J. Biol. Chem. *271*, 20246–20249.

Apgar, J., Tseng, Y., Federov, E., Herwig, M.B., Almo, S.C., and Wirtz, D. (2000). Multiple-particle tracking measurements of heterogeneities in solutions of actin filaments and actin bundles. Biophys. J. *79*, 1095–1106.

Arthur, W.T., and Burridge, K. (2001). RhoA inactivation by p190RhoGAP regulates cell spreading and migration by promoting membrane protrusion and polarity. Mol. Biol. Cell *12*, 2711–2720.

Arthur, W.T., Petch, L.A., and Burridge, K. (2000). Integrin engagement suppresses RhoA activity via a c-Src-dependent mechanism. Curr. Biol. *10*, 719–722.

Ballestrem, C., Hinz, B., Imhof, B.A., and Wehrle-Haller, B. (2001). Marching at the front and dragging behind: differential alphaVbeta3-integrin turnover regulates focal adhesion behavior. J. Cell Biol. *155*, 1319–1332.

Bausch, A.R., Hellerer, U., Essler, M., Aepfelbacher, M., and Sackmann, E. (2001). Rapid stiffening of integrin receptor-actin linkages in endothelial cells

stimulated with thrombin: a magnetic bead microrheology study. Biophys. J. *80*, 2649–2657.

Berg, H.C. (1993). Random Walks in Biology, Princeton, NJ: Princeton University Press.

Bishop, A.L., and Hall, A. (2000). Rho GTPases and their effector proteins. Biochem. J. *348*, 241–255.

Chandrasekhar, S. (1943). Stochastic problems in physics and astronomy. Rev. Mod. Phys. *15*, 1–89.

Chrzanowska-Wodnicka, M., and Burridge, K. (1996). Rho-stimulated contractility drives the formation of stress fibers and focal adhesions. J. Cell Biol. *133*, 1403–1415.

Crocker, J.C., Valentine, M.T., Weeks, E.R., Gisler, T., Kaplan, P.D., Yodh, A.G., and Weitz, D.A. (2000). Two-point microrheology of inhomogeneous soft materials. Phys. Rev. Lett. *85*, 888–891.

Dasgupta, B.R., Tee, S.Y., Crocker, J.C., Frisken, B.J., and Weitz, D.A. (2002). Microrheology of polyethylene oxide using diffusing wave spectroscopy and single scattering. Phys. Rev. E. Stat. Nonlin Soft Matter Phys. *65*, 051505.

Eckstein, A., Suhm, J., Friedrich, C., Maier, R.D., Sassmannshausen, J., Bochmann, M., and Mulhaupt, R. (1998). Determination of plateau moduli and entanglement molecular weights of isotactic, syndiotactic, and atactic polypropylenes synthesized with metallocene catalysts. Macromolecules *31*, 1335–1340.

Einstein, A. (1905). Über die von der molekularkinetischen Theorie der Wärme geforderte Bewegung von in ruhenden Flüssigkeiten suspendierten Teilchen. Ann. Physik *17*, 549

Ferry, J.D. (1980). Viscoelastic Properties of Polymers, New York: John Wiley & Sons.

Hall, A. (1998). Rho GTPases and the actin cytoskeleton. Science *279*, 509–514.

Hanks, S.K., Calalb, M.B., Harper, M.C., and Patel, S.K. (1992). Focal adhesion protein-tyrosine kinase phosphorylated in response to cell attachment to fibronectin. Proc. Natl. Acad. Sci. USA *89*, 8487–8491.

Heidemann, S.R., and Wirtz, D. (2004). Towards a regional approach to cell mechanics. Trends Cell Biol., *14*, 160–166.

Imamura, F., Mukai, M., Ayaki, M., and Akedo, H. (2000). Y-27632, an inhibitor of rho-associated protein kinase, suppresses tumor cell invasion via regulation of focal adhesion and focal adhesion kinase. Jpn. J. Cancer Res. *91*, 811–816.

Janmey, P.A., Hvidt, S., Lamb, J., and Stossel, T.P. (1990). Resemblance of actin-binding protein/actin gels to covalently networks. Nature *345*, 89–92.

Kaibuchi, K., Kuroda, S., and Amano, M. (1999). Regulation of the cytoskeleton and cell adhesion by the Rho family GTPases in mammalian cells. Annu. Rev. Biochem. *68*, 459–486.

Kimura, K., *et al*. (1996). Regulation of myosin phosphatase by Rho and Rho-associated kinase (Rho-kinase). Science *273*, 245–248.

Kozma, R., Ahmed, S., Best, A., and Lim, L. (1995). The Ras-related protein Cdc42Hs and bradykinin promote formation of peripheral actin microspikes and filopodia in Swiss 3T3 fibroblasts. Mol. Cell. Biol. *15*, 1942–1952.

Luby-Phelps, K. (1993). Physical properties of cytoplasm. Curr. Opin. Cell. Biol. *6*, 3–9.

Luby-Phelps, K. (2000). Cytoarchitecture and physical properties of cytoplasm: volume, viscosity, diffusion, intracellular surface area. Int. Rev. Cytol. *192*, 189–221.

Masiero, L., Lapidos, K.A., Ambudkar, I., and Kohn, E.C. (1999). Regulation of the RhoA pathway in human endothelial cell spreading on type IV collagen: role of calcium influx. J. Cell Sci. *112*, 3205–3213.

Mason, T.G., Ganesan, K., van Zanten, J.V., Wirtz, D., and Kuo, S.C. (1997). Particle-tracking microrheology of complex fluids. Phys. Rev. Lett. *79*, 3282–3285.

Mason, T.G., and Weitz, D. (1995). Optical measurements of frequency-dependent linear viscoelastic moduli of complex fluids. Phys. Rev. Lett. *74*, 1254–1256.

McGrath, J.L., Hartwig, J.H., Tardy, Y., and Dewey, C.F., Jr. (1998). Measuring actin dynamics in endothelial cells. Microsc. Res. Tech. *43*, 385–394.

Moolenaar, W.H. (1995). Lysophosphatidic acid signalling. Curr. Opin. Cell Biol. *7*, 203–210.

Nobes, C.D., and Hall, A. (1995). Rho, Rac, and Cdc42 Gtpases regulate the assembly of multimolecular focal complexes associated with actin stress fibers, lamellipodia, and filopodia. Cell *81*, 53–62.

Nobes, C.D., Hawkins, P., Stephens, L., and Hall, A. (1995). Activation of the small GTP-binding proteins rho and rac by growth factor receptors. J. Cell Sci. *108*, 225–233.

Pollard, T.D., Goldberg, I., and Schwarz, W.H. (1992). Nucleotide exchange, structure, and mechanical properties of filaments assembled from ATP-actin and ADP-actin. J. Biol. Chem. *267*, 20339–20345.

Qian, H., Sheetz, M.P., and Elson, E.L. (1991). Single particle tracking. Analysis of diffusion and flow in two-dimensional systems. Biophys. J. *60*, 910–921.

Ren, X.D., Bokoch, G.M., Traynor-Kaplan, A., Jenkins, G.H., Anderson, R.A., and Schwartz, M.A. (1996). Physical association of the small GTPase Rho with a 68-kDa phosphatidylinositol 4-phosphate 5-kinase in Swiss 3T3 cells. Mol. Biol. Cell *7*, 435–442.

Ren, X.D., Kiosses, W.B., and Schwartz, M.A. (1999). Regulation of the small GTP-binding protein Rho by cell adhesion and the cytoskeleton. EMBO J. *18*, 578–585.

Ren, X.D., Kiosses, W.B., Sieg, D.J., Otey, C.A., Schlaepfer, D.D., and Schwartz, M.A. (2000). Focal adhesion kinase suppresses Rho activity to promote focal adhesion turnover. J. Cell Sci. *113*, 3673–3678.

Ren, X.D., and Schwartz, M.A. (2000). Determination of GTP loading on Rho. Methods Enzymol. *325*, 264–272.

Ridley, A.J., and Hall, A. (1992). The small GTP-binding protein Rho regulates the assembly of focal adhesions and actin stress fibers in response to growth-factors. Cell *70*, 389–399.

Ridley, A.J., Paterson, H.F., Johnston, C.L., Diekmann, D., and Hall, A. (1992). The small GTP-binding protein Rac regulates growth-factor induced membrane ruffling. Cell *70*, 401–410.

Riveline, D., Zamir, E., Balaban, N.Q., Schwarz, U.S., Ishizaki, T., Narumiya, S., Kam, Z., Geiger, B., and Bershadsky, A.D. (2001). Focal contacts as mechanosensors: externally applied local mechanical force induces growth of focal contacts by an mDia1-dependent and ROCK-independent mechanism. J. Cell Biol. *153*, 1175–1186.

Rottner, K., Hall, A., and Small, J.V. (1999). Interplay between Rac and Rho in the control of substrate contact dynamics. Curr. Biol. *9*, 640–648.

Sato, M., Schwarz, W.H., and Pollard, T.D. (1987). Dependence of the mechanical properties of actin/alpha-actinin gels on deformation rate. Nature *325*, 828–830.

Schmidt, A., and Hall, M.N. (1998). Signaling to the actin cytoskeleton. Annu. Rev. Cell Dev. Biol. *14*, 305–338.

Seufferlein, T., and Rozengurt, E. (1994). Lysophosphatidic acid stimulates tyrosine phosphorylation of focal adhesion kinase, paxillin, and p130. Signaling pathways and cross-talk with platelet-derived growth factor. J. Biol. Chem. *269*, 9345–9351.

Sinnett-Smith, J., Lunn, J.A., Leopoldt, D., and Rozengurt, E. (2001). Y-27632, an inhibitor of Rho-associated kinases, prevents tyrosine phosphorylation of focal adhesion kinase and paxillin induced by bombesin: dissociation from tyrosine phosphorylation of p130(CAS). Exp. Cell Res. *266*, 292–302.

Suh, J., Wirtz, D., and Hanes, J. (2003). Efficient active transport of gene nanocarriers to the cell nucleus. Proc. Natl. Acad. Sci. USA *100*, 3878–3882.

Theriot, J.A., and Mitchison, T.J. (1991). Actin microfilament dynamics in locomoting cells. Nature *352*, 126–131.

Tilney, L.G., Connelly, P.S., Vranich, K.A., Shaw, M.K., and Guild, G.M. (2000). Regulation of actin filament cross-linking and bundle shape in *Drosophila* bristles. J. Cell Biol. *148*, 87–100.

Tseng, Y., An, K.M., and Wirtz, D. (2002a). Microheterogeneity controls the rate of gelation of actin filament networks. J. Biol. Chem. *277*, 18143–18150.

Tseng, Y., Kole, T.P., and Wirtz, D. (2002b). Micromechanical mapping of live cells by multiple-particle-tracking microrheology. Biophys. J. *83*, 3162–3176.

Tseng, Y., and Wirtz, D. (2001). Mechanics and multiple-particle tracking microheterogeneity of alpha-actinin-cross-linked actin filament networks. Biophys. J. *81*, 1643–1656.

Tsubouchi, A., Sakakura, J., Yagi, R., Mazaki, Y., Schaefer, E., Yano, H., and Sabe, H. (2002). Localized suppression of RhoA activity by Tyr31/118-phosphorylated paxillin in cell adhesion and migration. J. Cell Biol. *159*, 673–683.

Van Aelst, L., and D'Souza-Schorey, C. (1997). Rho GTPases and signaling networks. Genes Dev. *11*, 2295–2322.

Watanabe, N., Kato, T., Fujita, A., Ishizaki, T., and Narumiya, S. (1999). Cooperation between mDia1 and ROCK in Rho-induced actin reorganization. Nat. Cell Biol. *1*, 136–143.

Xu, J., Viasnoff, V., and Wirtz, D. (1998a). Compliance of actin filament networks measured by particle-tracking microrheology and diffusing wave spectroscopy. Rheologica Acta *37*, 387–398.

Xu, J., Wirtz, D., and Pollard, T.D. (1998b). Dynamic crosslinking by α-actinin determines the mechanical properties of actin filament networks: J. Biol. Chem. *273*, 9570–9576.